

## Supporting Information

### Highly effective bifunctional defective cobalt phthalocyanine for photo-involved lithium-oxygen batteries

Yujiao Xia<sup>a</sup>, Xingyu Yu<sup>a</sup>, Yunyun Xu<sup>a</sup>, Xiaoli Fan<sup>b, \*</sup>, Bin Gao<sup>c</sup>, Cheng Jiang<sup>a</sup>, Mingyue Zhang<sup>a</sup>,  
Xianli Huang<sup>a</sup>, Hao Gong<sup>d, \*</sup>, Jianping He<sup>a</sup>, Tao Wang<sup>a, \*</sup>

<sup>a</sup> Centre for Hydrogenenergy, Jiangsu Key Laboratory of Materials and technology for Energy Conversion, College of Materials Science and Technology, Nanjing University of Aeronautics and Astronautics, Nanjing 210016, PR China

<sup>b</sup> School of Materials Science and Engineering, Nanjing Institute of Technology, Nanjing 211167, P. R. China

<sup>c</sup> Jiangsu Key Laboratory for Nano Technology, College of Engineering and Applied Sciences, Nanjing University, Nanjing 210093, PR China

<sup>d</sup> Department of Chemistry and Materials Science, College of Science, Nanjing Forestry University, Nanjing 210037, PR China

#### Experimental Section

##### Materials

Carbon nanotubes (CNTs,  $\geq 95\%$ ), anhydrous cobalt chloride ( $\text{CoCl}_2$ , 99.0%), 1,8-diazodicyclic [5.4.0] undecylcarbon-7-ene (DBU, 99.0%), 1,2-dicyanobenzene ( $\text{C}_8\text{H}_4\text{N}_2$ , 98%), 1,2,4,5-tetracyanophenyl benzene (TCNB, 97%), Super P, bis(trifluoromethane)sulfonimide lithium salt (LiTFSI,  $\geq 99\%$ ), tetraethylene glycol dimethyl ether (TEGDME, 99%) and 1-methyl-2-pyrrolidinone (NMP,  $>99.0\%$ ) were purchased from Aladdin Chemistry Co., LTD. Polyvinylidene fluoride (PVDF,  $\sim 400000$ ) was purchased from McLean Chemical Reagent Co., LTD. Nitric acid ( $\text{HNO}_3$ , 68%) and ethanol ( $\text{C}_2\text{H}_5\text{OH}$ ,  $>99.0\%$ ) were purchased from Sinopharm Group Chemical reagent Co., LTD. All chemicals used in the experiment are analytical reagent and have not been pre-treated before used.

##### Synthesis of acidified carbon nanotubes (O-CNTs)

0.5 g CNTs were added to 50 mL  $\text{HNO}_3$ , reflowed for 3 h at 100 °C, and then cleaned with deionized water to make the solution neutral. After separation of solid

and liquid by centrifugal procedure, the black powder was dried for 12h under vacuum condition of 60°C, and O-CNTs were obtained after full grinding.

### **Synthesis of D-CoPPc/CNT**

In the general synthesis process, 50 mg O-CNTs were added in 40 mL ethanol and ultrasound for 30 min. Then 18 mg CoCl<sub>2</sub>, 43 mg DBU, 16 mg phthalonitrile and 34 mg TCNB were added to the mixed solution for additional 30 min ultrasound. The mixture was then packed in 100ml Teflon-autoclave and heated at 180°C, then held it at that temperature for 8 h. After the reaction, the product was separated by centrifugation at a rotational speed of 8000 r/min, while ethanol and water were used as cleaning agents, and then vacuum drying at 60°C for 12 h. D-CoPPc/CNT with mass ratios of 4:1, 2:1 and 1:1 of TCNB and phthalonitrile were prepared, which were named as D4-CoPPc/CNT, D2-CoPPc/CNT and D1-CoPPc/CNT, respectively.

Carbon nanotubes supported polymerized cobalt phthalocyanine (CoPPc/CNT) and carbon nanotubes supported cobalt phthalocyanine (CoPc/CNT) were prepared by a same process with no additional phthalonitrile and TCNB, respectively.

### **Characterization**

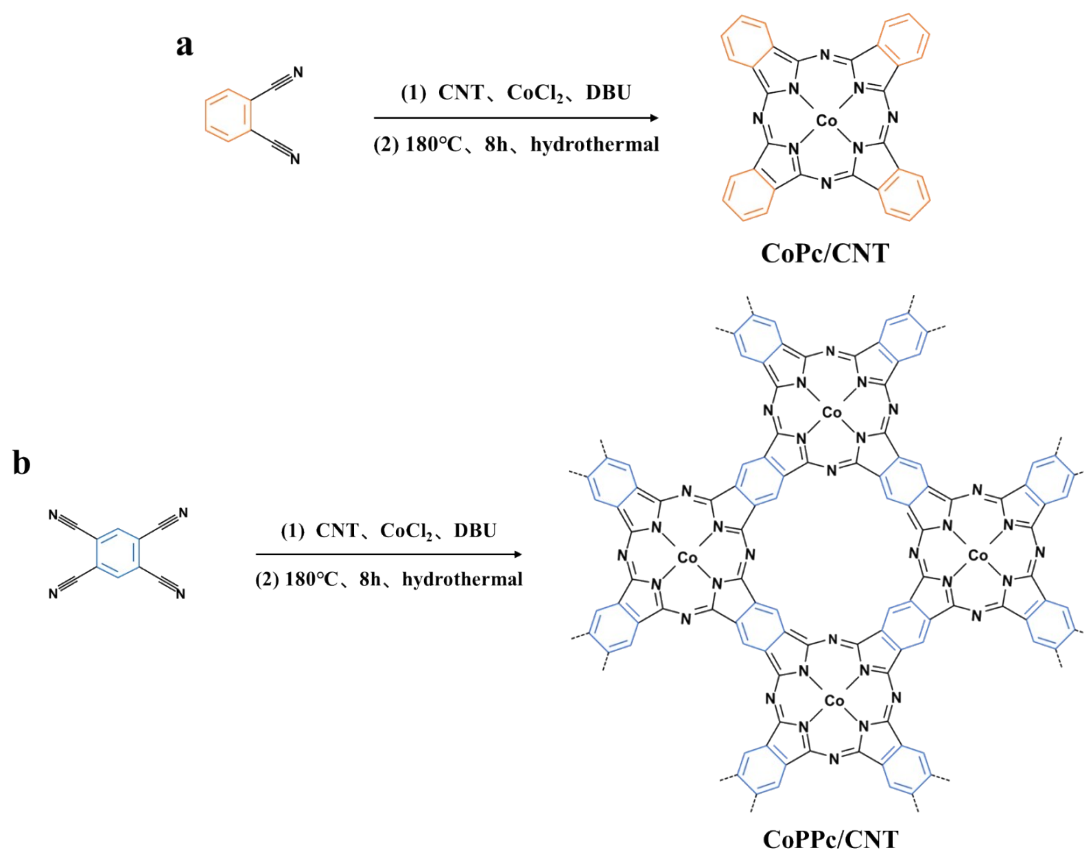
The determination of the material structure depends on X-ray diffraction (XRD, Bruker D8 Advance Eco) using Cu K $\alpha$  radiation ( $\lambda = 1.5418 \text{ \AA}$ ), and the test was performed at a sweep speed of 5° min<sup>-1</sup> in the range of 5~85°. The morphology and elemental distributions were observed with scanning electron microscopy (SEM, LYRA3 GMU) and High-resolution transmission electron microscope (HR-TEM, FEI Tecnai G2F20 microscope) with an energy dispersive X-ray spectroscopy (EDS) detector. The chemical composition of the samples was measured through Raman spectrometer (Raman, HORIBA Scientific LabRAM HR Evolution) and Fourier transform infrared spectrometer (FT-IR, Thermo Scientific Nicolet iS20). The chemical elements of the materials and the states can be derived from X-ray photoelectron spectrometer (XPS, Thermo Scientific K-Alpha, Al K $\alpha$  illumination,  $\lambda = 1486.6 \text{ eV}$ ). The UV-vis spectra were displayed on Shimadzu UV-3600. The steady-state photoluminescence (PL) spectra were obtained on a Horiba Fluorolog-3-TCSPC spectrophotometer with an excitation wavelength of 360 nm. The specific surface area

measurement was tested by a 4-station automatic specific surface area analyzer (Micrometrics Instrument Corporation, ASAP 2460). Inductively coupled plasma mass spectrometry (ICP-MS) was performed on a Thermo Fisher iCAP PRO instrument.

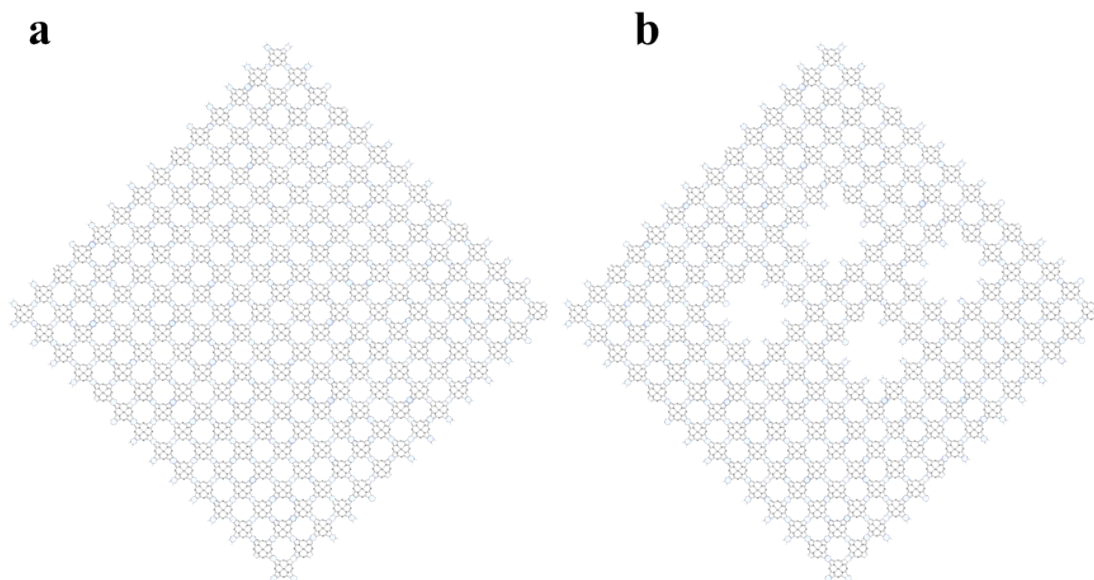
### **LOB assembly and electrochemical measurement**

The oxygen cathode was obtained by dropping a prepared grout onto a 12mm diameter piece of carbon paper. Firstly, D-CoPPc/CNT, PVDF and Super P were added into NMP according to the mass ratio of 8:1:1. After 30 min of ultrasound, a uniform catalyst ink was obtained. Then it was dripped onto the carbon paper, ensuring that the load on each sheet was 0.2 mg. After vacuum drying at 60°C for 12 h, it was quickly placed in a glove box full of Ar ( $\text{H}_2\text{O} < 0.01$  ppm,  $\text{O}_2 < 0.01$  ppm) for battery assembly in a homemade unit. The cathode of the battery is lithium metal, the separator is fiberglass, and the electrolyte is a 1 M LiTFSI/TEGDME mixture. After the battery was assembled,  $\text{O}_2$  (99.999%) was injected into the device for 10 min to ensure that the device was full of pure oxygen. With an optical source of 300 W Xe lamp (PLS-SXE300C, Perfect-Light, Beijing), the charge-discharge curve test of the battery was performed on CT2001A LAND Battery Test System (Wuhan, China).

Most of the photoelectron-chemistry tests were performed on the Zahner electrochemical workstation. Linear sweep voltammetry (LSV) curves of ORR process were recorded by scanning negatively over the voltage ranges of 2.5~3.1 V. In OER process, LSV curves were recorded by scanning forward over the voltage ranges of 3.1~4.0 V. The chronoamperometry (I-t) curves were performed by chopping light every 60 s over a period of 0~600 s. The constant potential was set to 2.8 V during discharge and 3.7 V during charge. The electrochemical impedance spectroscopy (EIS) profiles were logged in the 100 kHz-100 mHz frequency range. The Mott-Schottky plots were measured in a three-electrode system (D-CoPPc/CNT as work electrode, calomel saturation electrode as reference electrode and platinum electrode as counter electrode). On CHI 660E workstation, the cyclic voltammetry (CV) curves were measured at a sweep speed of 1 mV s<sup>-1</sup> over a working window range of 2~4.5 V.



Scheme S1. The synthetic pathways of (a) CoPc and (b) CoPPc/CNT.



Scheme S2. The structure schematic diagrams of (a) CoPPc and (b) D-CoPPc.

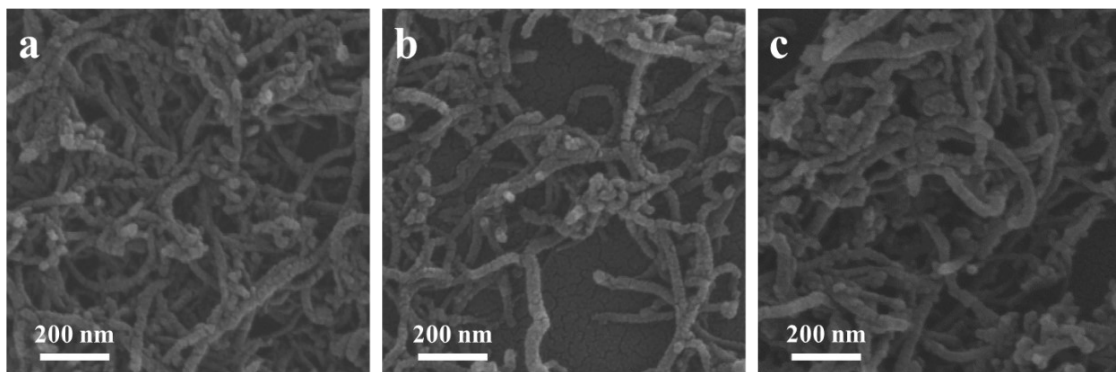


Figure S1. SEM images of (a) CNT, (b) CoPPc/CNT, (c) D-CoPPc/CNT.

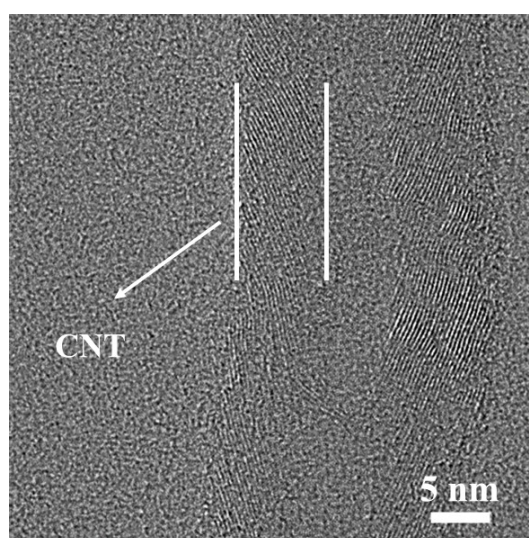


Figure S2. The TEM image of CNT.

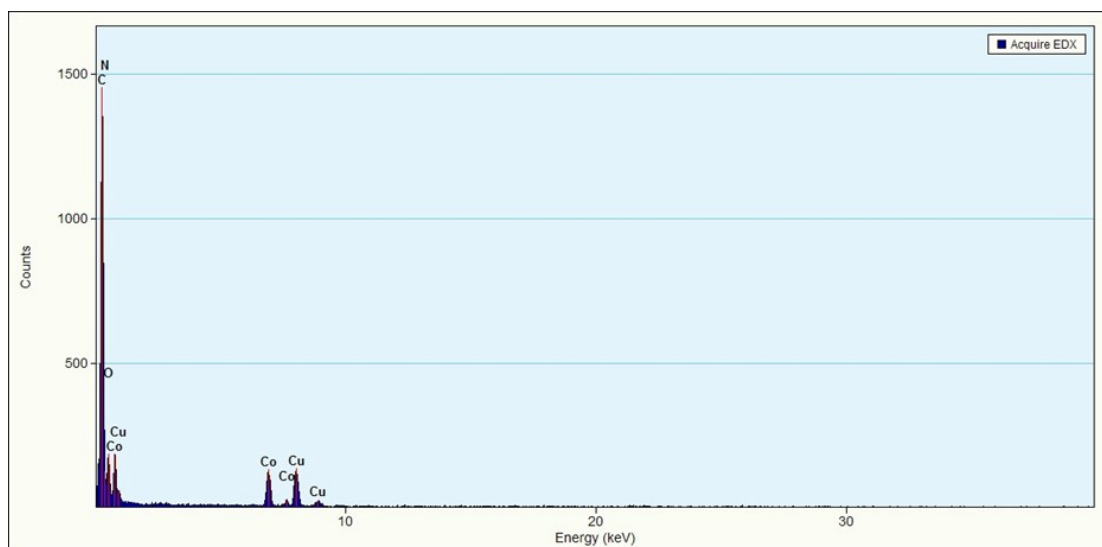


Figure S3. Energy dispersive X-Ray spectroscopy (EDX) energy spectrum of D-CoPPc/CNT.

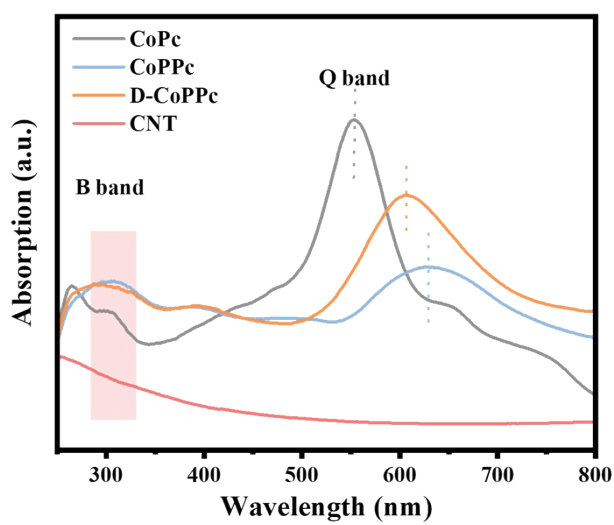


Figure S4. UV-vis spectra of CoPc, CoPPc, D-CoPPc and CNT.

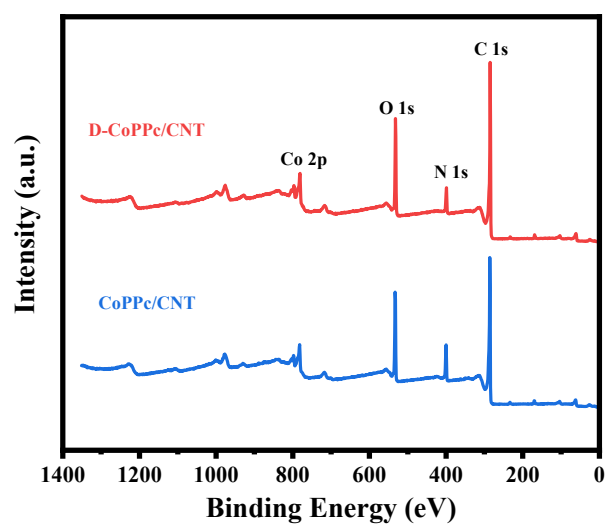


Figure S5. XPS survey spectra of D-CoPPc/CNT and CoPPc/CNT.

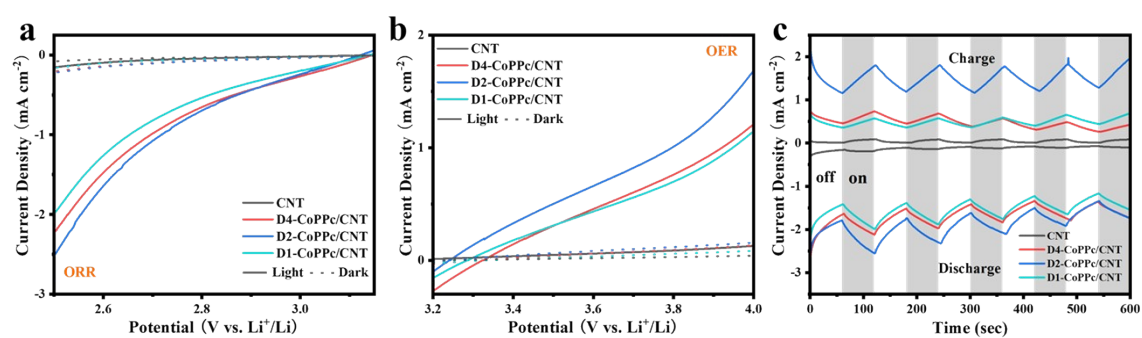


Figure S6. LSV curves of CNT, D4-CoPPc/CNT, D2-CoPPc/CNT and D1-CoPPc/CNT with light or dark in (a) ORR process, (b) OER process. (c) I-t curves of CNT, D4-CoPPc/CNT, D2-CoPPc/CNT and D1-CoPPc/CNT with a chopping light every 60 seconds.

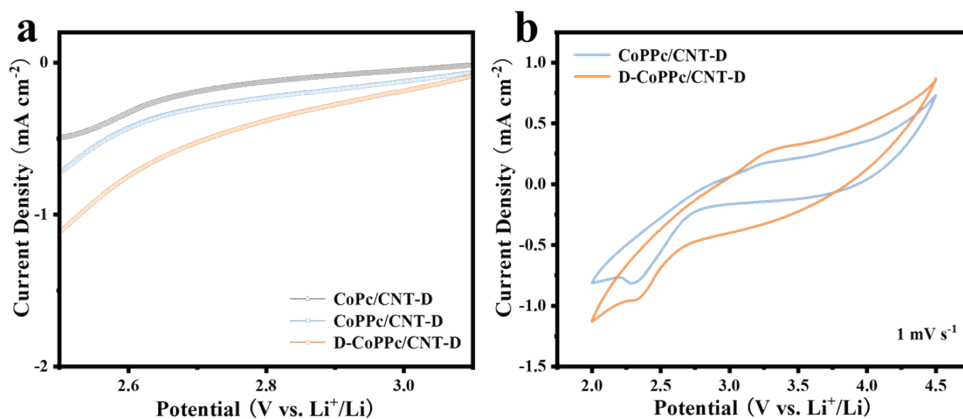


Figure S7. (a) LSV curves of CoPc/CNT, CoPPc/CNT and D-CoPPc/CNT in dark during ORR process. (b) CV curves of D-CoPPc/CNT and CoPPc/CNT in dark at a scan rate of 1 mV s<sup>-1</sup>.

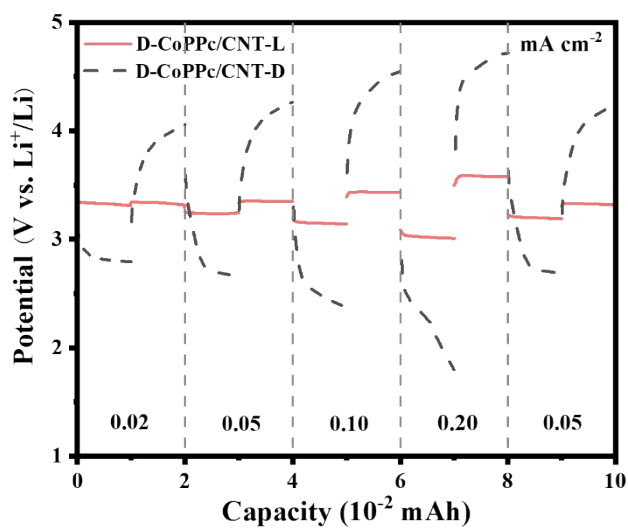


Figure S8. Rate performance of the Li-O<sub>2</sub> battery with D-CoPPc/CNT as an oxygen cathode with and without illumination.



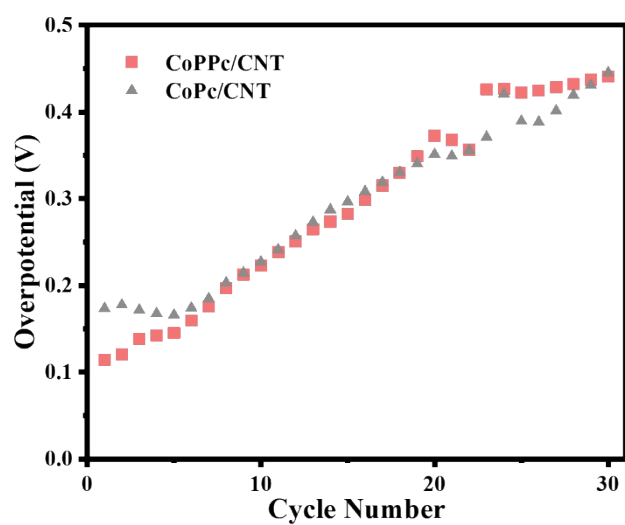


Figure S9. Overpotential of the battery change with the cycle number in the first 30 cycles with CoPPc/CNT and CoPc/CNT as oxygen cathodes without illumination.

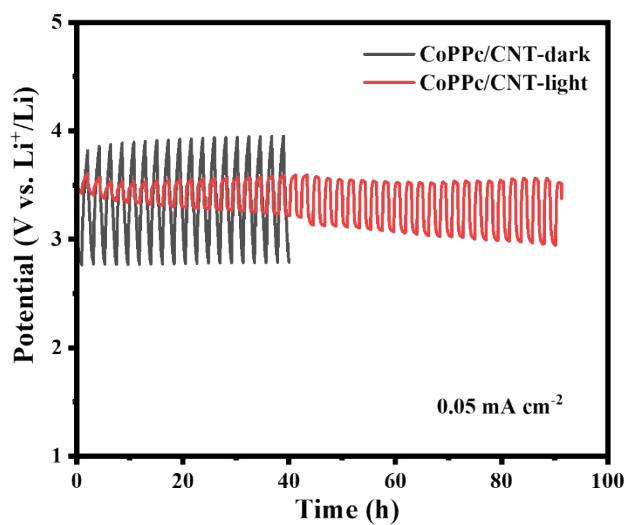


Figure S10. Discharge–charge cycles with CoPPc/CNT as an oxygen cathode at a current density of  $0.05 \text{ mA cm}^{-2}$  in light and dark.

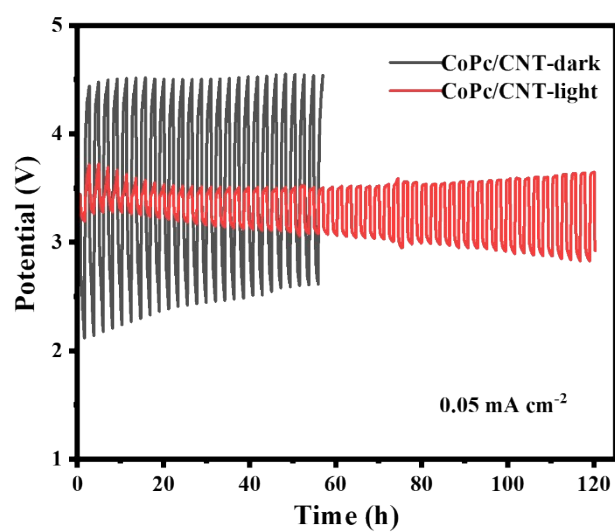


Figure S11. Discharge–charge cycles with CoPc/CNT as an oxygen cathode at a current density of  $0.05 \text{ mA cm}^{-2}$  in light and dark.

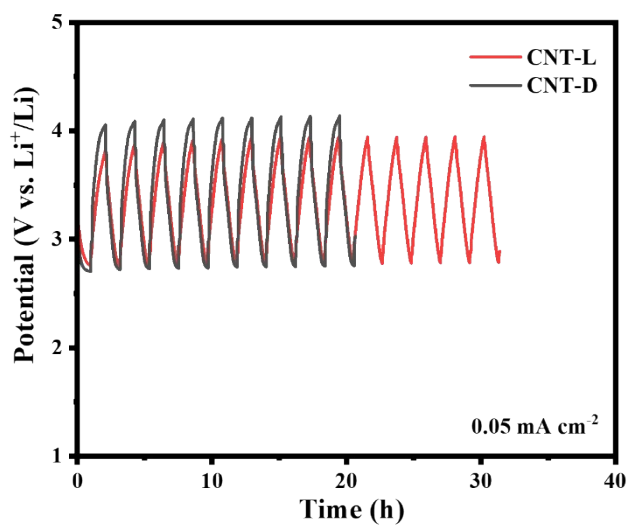


Figure S12. Discharge–charge cycles with CNT as an oxygen cathode at a current density of  $0.05 \text{ mA cm}^{-2}$  in light and dark.

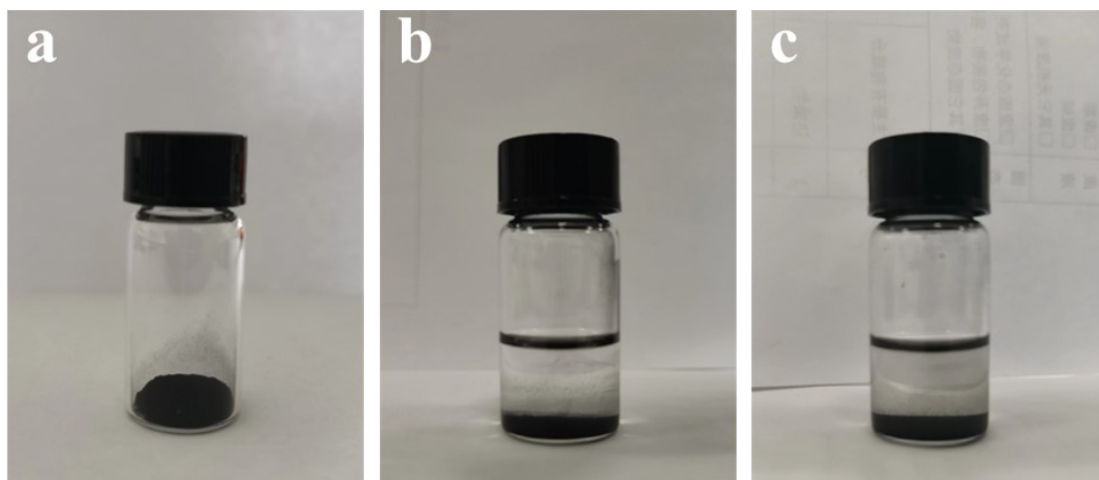


Figure S13. (a) D-CoPPc/CNT powder. D-CoPPc/CNT was soaked in 1 M LiTFSI/TEGDME the solution for (b) 0 h and (c) 24 h.

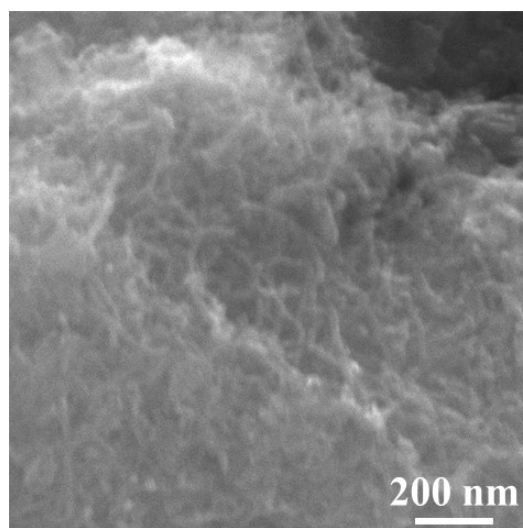


Figure S14. SEM image of D-CoPPc/CNT cathode at pristine state.

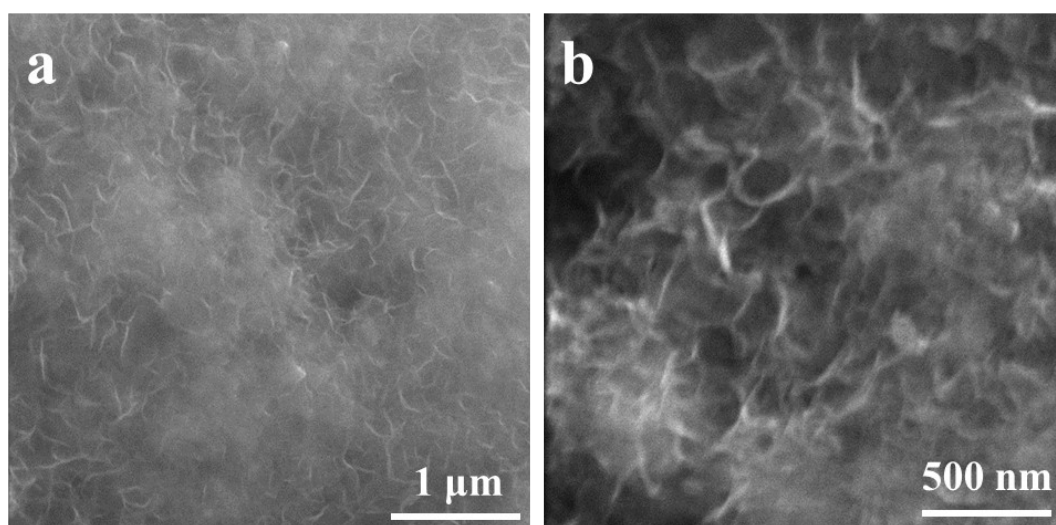


Figure S15. (a) (b) SEM images of D-CoPPc/CNT cathode at discharge state.

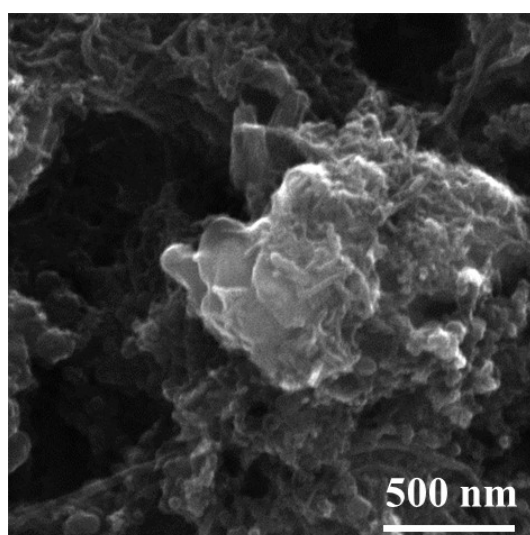


Figure S16. SEM image of D-CoPPc/CNT cathode at recharge state.

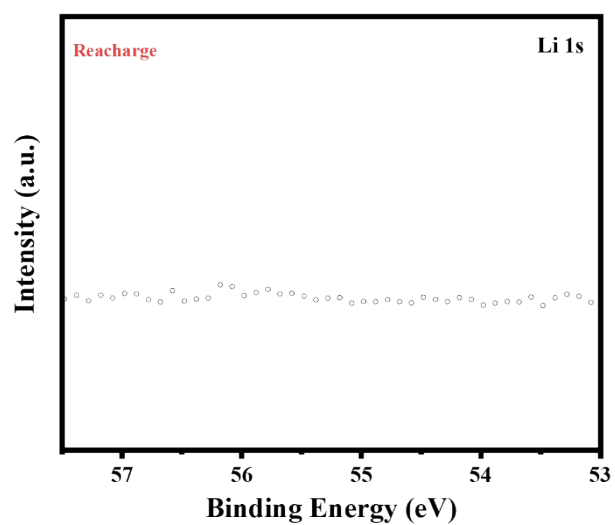


Figure S17. XPS spectrum of Li 1s after recharge.

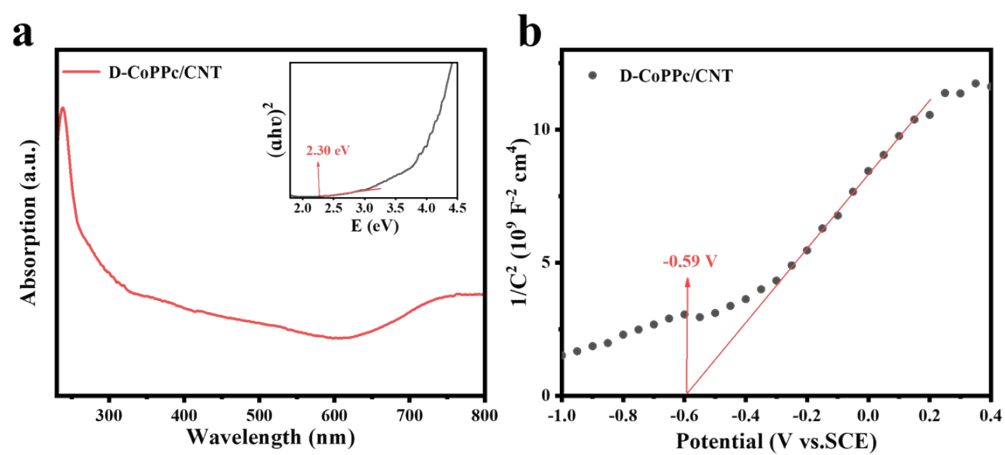


Figure S18. (a) UV-vis spectra of D-CoPPc/CNT. The inset shows the Tauc plot converted from the UV-vis spectra. (b) Mott-Schottky plot of D-CoPPc/CNT at 2 kHz.

Table S1 Comparison of the performance in this study with some previously reported work in a photo-assisted LOB system.

Cathode	Electrolyte	Discharge/Charge potential (V)	Current density (mA cm <sup>-2</sup> )	Energy efficiency (%)	Ref.
D-CoPPc/CNT	aprotic	3.30 / 3.40	0.05	97.1	<b>This work</b>
TiO <sub>2</sub> /Fe <sub>2</sub> O <sub>3</sub>	aprotic	3.01 / 3.20	0.01	94.1	<i>Adv.Mater.</i> <b>2020</b> , 32, 1907098
b-TiO <sub>2</sub> /CC	aprotic	2.87 / 3.13	0.01	91.7	<i>Nano Energy</i> <b>2022</b> , 98, 107248
NiO/FNi	aprotic	2.63 / 2.92	0.01	90.1	<i>Adv.Mater.</i> <b>2022</b> , 34, 2104792
WO <sub>3</sub> @g-C <sub>3</sub> N <sub>4</sub> NWA	aprotic	2.76 / 3.69	0.10	74.8	<i>Nanoscale</i> <b>2020</b> , 12,18742–18749
MoS <sub>2</sub> /ZnIn <sub>2</sub> S <sub>4</sub>	aprotic	3.18 / 3.29	0.05	96.7	<i>Carbon Energy</i> <b>2022</b> , 4, 1169–1181
Co-TABQ	aprotic	3.12 / 3.32	0.10	94.0	<i>J. Am. Chem. Soc.</i> <b>2021</b> , 143, 1941-1947
Au-Nv-C <sub>3</sub> N <sub>4</sub>	aprotic	3.16 / 3.26	0.05	97.0	<i>PNAS</i> <b>2021</b> , 118, e2024619118